Enhancing Solar Air Heater Heat Transfer Performance: The Impact of Hexagonal 90° and 120° Inline Ribs with Varying Blockage Ratios in Trapezoidal Ducts

Nilesh M. Shinde[1], Dr. Himanshu Borade[2]
[1]Department of Mechanical Engineering, Medi-Caps University, Indore, India,
[2]Department of Mechanical Engineering, Medi-Caps University, Indore, India [1]nmshinde@outlook.com,
[2]himanshu.borade@medicaps.ac.in

Abstract*—An experimental investigation was carried out to evaluate the thermo-hydraulic performance of a solar air heater (SAH) equipped with a hexagonal ribbed absorber plate. The study examines the effects of geometric parameters—blockage ratio (e/Dh = 0.1109, 0.1479, and 0.1849), rib pitch (P = 60 mm, 80 mm, and 100 mm), and angle of attack (α = 90° and 120°) on heat transfer and flow dynamics within a trapezoidal duct, over a Reynolds number range of 5000 to 30,000. Trapezoidal ducts were selected for their ability to enhance surface area and flow interaction. For Reynolds numbers ranging from 5000 to 30,000, the Nusselt number for α = 90° inline ribs increased by 20–40%, while the α = 120° inline ribs exhibited a higher enhancement of 40–60%. This improvement in heat transfer was accompanied by an increase in flow resistance. The friction factor for α = 90° ribs was about 1.5–2.0 times higher than the smooth duct, whereas for α = 120° ribs it increased by nearly 2.5–3.0 times. Considering both parameters, the thermo-hydraulic performance factor (TPF) was found to be superior for the α = 120° configuration, ranging from 1.09 to 1.29, compared to 1.01 to 1.11 for the α = 90° case. This suggests that higher angles and blockage ratios enhance turbulence and mixing, improving heat transfer with manageable pressure losses. Overall, the hexagonal ribbed absorber significantly improves thermal efficiency, offering a promising and cost-effective solution for enhancing solar air heater performance while supporting energy efficiency and environmental sustainability.

Keywords— Convective heat transfer, blockage ratio, heat transfer raise, artificial roughness, and hexagonal ribs.

I. INTRODUCTION

To meet their energy needs and promote economic progress, nations must look for alternate alternatives as renewable energy sources become less available. Solar energy, also known as insolation, which is produced by the sun's rays, is one viable alternative. This renewable natural resource can be used directly or converted into various types of energy, making it a cost-effective, environmentally responsible, and adaptable power source. Not only is solar energy reliable and plentiful, but it also has some environmental impact. Humanity has created several inventive methods over the ages to efficiently harvest and use solar energy for daily needs [1–3].

Applying artificial geometry to the surface is an excellent method to improve heat transfer to the air flowing through the duct. Numerous studies have proposed enhancing the heat transfer coefficient by incorporating roughness using ribs and wires of various sizes, shapes, and characteristics. Roughness geometry has been employed to enhance the heat transfer coefficient by inducing turbulence and flow disturbances. Consequently, such geometry will lead to increased frictional losses, thereby elevating the power required to transport air through the duct. Turbulence should be generated solely in the vicinity of the duct layer, specifically within the laminar sublayer, to minimize frictional losses. The structure and characteristics of roughness on the absorber plate are influenced by several factors. The height (e) and pitch (p) of the roughness elements are the primary factors. Dimensionless parameters, such as e/D, representing the ratio of roughness element height to hydraulic duct diameter, and p/e, are commonly employed to articulate these characteristics. The elements of roughness may include V-shaped, angled, two-dimensional transverse, or discrete rib configurations, among other forms. While square and circular ribs are predominant, protruded, grooved, and chamfered geometries have also been examined as elements of roughness. Nikuradse conducted the preliminary inquiry into the influence of roughness on flow, executing multiple investigations utilizing pipes roughened with sand grains to assess the impact of roughness on the friction factor and velocity distribution [4].

Agarwal et al. [5] conducted a study on discrete double-arc ribs and observed that the friction factor and Nusselt number exhibited enhancements of approximately 3.07 and 3.17 times, respectively, when compared to the smooth case. Chabane et al. [6] conducted an examination of how the positioning of transverse continuous rectangular baffles affects outcomes. Baffles were installed on 30% of the absorber plate in the upstream section, 30% in the center section, and 30% in the downstream section. The addition of baffles to 30% of the middle absorber plate resulted in an increase in thermal efficiency and a reduction in pressure drop. When the height was set at 0.1 and the relative pitch at 1.0, the maximum THPP recorded was 1.87. The maximum THPP for continuous V-shaped baffles was recorded at 2.25, while for discrete V-shaped baffles, it reached 2.69, as indicated by research examining the impact of pitch on both baffle types [7]. Ribs, which are three-dimensional structures, exhibit various cross-sectional shapes. These include circular [8], rectangular [9,10], trapezoidal [9, 11,12], triangular [9,13,14], inverted T [15], polygonal [11], reverse NACA profile [16], pentagonal [17], and D-shaped [18]. The maximum value of THPP for each rib shape was documented, and the influence of rib factors, including

height and pitch, on THPP was analysed. The maximum THPP for pentagonal ribs [17] and reverse NACA profile ribs [16] varied between 1.46 and 2.65. In addition to straight transversal ribs, V-shaped transversal ribs have also been the subject of study. The performance of an SAH has been analysed concerning the geometrical characteristics of V-shaped ribs, which include height, pitch, angle of attack, and the number of transversal V-ribs.

An assessment of the influence of the angle of attack on a single transversal V-rib [19] indicates that the optimal angle of attack is 45°, resulting in a THPP of 2.01 [19]. Hans et al. [20] assessed the impact of the angle of attack and the quantity of transversal V-ribs, revealing that the optimal values for these parameters were determined to be 60° and six, respectively. Jin et al. [21] evaluated the impact of the angle of attack, the quantity of transversal V-ribs, and various geometrical features of V-shaped ribs. Researchers have established an optimal number of transversal V-ribs for each angle of attack. The configuration included seven transversal V-ribs and a 45° angle of attack, resulting in a maximum THPP of 2.35. Discrete elements, characterized by their three-dimensional structures, are distributed throughout the absorber plate. The subsequent elements have undergone analysis: The study has examined various types of discrete elements, including delta-shaped [22], cubical [23], stepped cylindrical [24], helicoidal spring [25], truncated half canonical [26], C-shaped [27,28], cylindrical [29,30], conical [31], frustum [32], and spherical ball [33]. Research has been carried out to examine the impacts of height, length, transversal pitch, and longitudinal pitch. The maximum value of THPP for truncated half canonical elements was adjusted from 1.20, as observed in cylindrical elements, to 2.04.

Further research on diverse roughness geometries is crucial for enhancing the heat transfer and overall efficiency of SAH. While various roughness configurations have shown promise, further investigation is necessary to assess their performances, understand the underlying mechanisms, and determine the optimal designs. Investigating and refining these geometries can significantly enhance the efficacy and efficiency of SAH, contributing to the development of sustainable energy solutions.

A. Objective of study

The main objective of this study is to experimentally investigate the influence of Hexagonal shaped rib roughness on the thermal and hydraulic performance of a trapezoidal duct solar air heater. Specifically, the study aims to analyse the variations in heat transfer coefficient and friction factor induced by the roughness elements and to compare the results with those obtained for a smooth absorber surface. Additionally, the work seeks to assess the overall improvement in thermo-hydraulic performance achieved through the use of hexagonal shaped ribs. In the present experimental study, the geometry of a hexagonal shaped obstacle is employed in the path of fluid flow, resulting in an improvement in thermo-hydraulic performance and efficiency. The trapezoidal duct exhibiting forced convection heat transfer phenomenon represents the simplest & most efficient phenomenon to enrich heat transfer and improve thermo-hydraulic performance.

This can be achieved by inducing roughness geometries of various sizes and shapes. The effectiveness of this improvement is contingent upon numerous parameters, namely rib diameter, pitch of the roughness component, angle of attack & the value of Reynolds number. Additionally, the operating parameters encompass temperature at the inlet & outlet, and flow conditions. Roughness geometry is situated between the working fluid & absorber plate. The thermal resistance for the heat flow due to convection is primarily induced by the viscous sublayer that develops near the heat transfer surface. The introduction of artificial roughness not only greatly improves the heat transfer coefficient but also increases losses that occur to overcome friction, which in turn demands more power to move the working fluid (air) through the duct. As a result, optimising the geometric values of the roughness is crucial to maximise heat transfer benefits while minimising the negative impact of higher frictional losses.

TABLE I. A COMPARATIVE ANALYSIS OF THIS WORK'S OUTCOMES AGAINST SIMILAR STUDIES, HIGHLIGHTING KEY DIFFERENCES AND PERFORMANCE IMPROVEMENTS.

Sr. No	Reynolds Number	Angle of Attack	Shape	Result	Ref.
1	3010-13935	α = 30°-75°	Double-arc ribs	THP 2.824.	[5]
2	5000-10000	-	Rectangular Baffles	η=88% for mode-2	[6]
3	6000-14000	-	Inclined baffles	THP 2.69	[7]
4	5000-30000	α = 50◦	Wire-shaped	THP 1.148	[8]
5	4000-16000	α = 90◦, 45◦	V-shaped ribs	45 V-shaped more THP	[10]
6	3800-18000	-	Trapezoidal & Polygonal	THP 1.89	[11]
7	2000-16000	α = 60°	Trapezoidal ribs	THP 3.24–3.79.	[12]
8	2000-20000	-	V shape	η=75.31%	[14]
9	3800-18000	α = 90°	Inverted-T shaped	THP 1.87	[15]
10	6000-18000	α = 30°	NACA profile ribs	THP 2.578	[16]
11	4000-15000	-	Pentagonal rib	THP 1.46	[17]
12	10200- 20200	-	D-shaped rib	THP 1.12	[18]
13	5000-20000	α = 45°	V-rib	ηex=23%	[19]
14	2000-20000	α =30–75°	V-rib	THP max at P/e=8	[20]
15	2100-30000	α = 30° to 90°	Delta shaped	THP max at Pl/e=3/2	[23]
16	3000-8000	-	Cubical rib	Nu= 59.1–72.7%	[24]
17	3000-24000	-	Stepped cylindrical rib	THP 1.49	[25]
18	3000-27000	-	C-shape fin	THP max at P/g ratio, 3.8	[27]
19	4000-18000	-	C-Shape, R-Shape	THP 2.0078	[28]

B. Reason for choosing hexagonal shaped geometry and parameter

The selection of hexagonal geometry is based on its capacity to significantly boost heat transfer in solar air heating systems. The unique sharp edge of this configuration disrupts the flow pattern by causing repeated separation and reattachment zones, intensifying turbulence around the absorber surface. This increased turbulence enhances convective heat transfer by thinning the thermal boundary layer. Moreover, the hexagonal encourages secondary flows

that improve fluid mixing and promote uniform temperature distribution. Although this design may lead to a higher-pressure drop, the trade-off is justified by a notable gain in overall thermo-hydraulic efficiency. Additionally, its structural adaptability—such as the ability to adjust pitch, shape, and orientation—makes it suitable for system-specific performance optimization. The selection of roughness geometric parameters has been carefully determined based on multiple critical factors, including insights from previous research, thermohydraulic performance optimization, constraints related to fabrication feasibility, and the typical Reynolds number range applicable to solar air heaters. These considerations guided the choice of parameter ranges that can enhance heat transfer effectively while keeping the pressure drop within acceptable limits. The specific values and ranges used in this study are presented in Table II

C. Novelty and scope of the present study

Novelty and scope of the present study Although similar roughness geometries have been examined in earlier studies, the present work contributes several distinct advancements. This investigation spans a broader Reynolds number range (5000–30,000) and applies a novel combination of surface roughness parameters, such as a relative pitch (p/e) of 10 and a relative height (e/Dh = 0.1109, 0.1479, and 0.1849), angle of attack (α = 90°,120°). A systematic evaluation of varying is undertaken, offering detailed insights that have not been thoroughly addressed in previous research. The experimental setup features a high aspect ratio duct (W/H = 10.57) and employs precisely calibrated instruments to enhance measurement reliability. An aluminium absorber plate, a consistent test section length of 1 m, and thermally efficient polystyrene insulation are incorporated to maintain experimental consistency. These carefully chosen parameters and configurations enable a deeper understanding of how hexagonal shaped roughness influences thermohydraulic performance in solar air heaters.

TABLE II. OPERATING PARAMETERS FOR EXPERIMENT

Parameters	Values
Reynolds No. (Re)	5000-30000
Ratio of p/e	10
Ratio of e/Dh	0.1109, 0.1479 and 0.1849
Angle of arc (α)	90°,120°
Duct aspect ratio, W/H	10.57
Hydraulic diameter, Dh	0.05408
Pitch of roughness profile, p	60 mm,80 mm, and 100 mm
Roughness diameter, e	6 mm, 8 mm, and 10 mm
Incident heat flux, I	1000 W/m2
Plate material	Aluminium
Test section length	1 m

II. EXPERIMENTAL TESTING OF A SOLAR AIR HEATER

An experimental framework has been designed and constructed to investigate the effects of hexagonal ribs on fluid flow characteristics and heat transfer in a trapezoidal duct, considering operating conditions and realistic system parameters, in accordance with ASHRAE standards (1977) (Figs. 1, 2, and 3). The experimental duct consists of a wooden conduit divided into three segments: an entrance segment, a test segment, and an exit segment. The absorber plate consists of aluminum grade 6063, exhibiting a thermal conductivity of 201-218 W/mK. Its dimensions are 1.0 m in length, 0.3 m in width, and 0.03 m in height. The lower surface of the sheet features artificially roughened hexagonal ribs exhibiting varying blockage ratios. Two halogen bulbs, each rated at 500 watts, are employed to generate a consistent heat flux of 1000 W/m². Figures 1 and 3 illustrate the block diagram of the experimental setups and the hexagonal rib configuration, respectively.

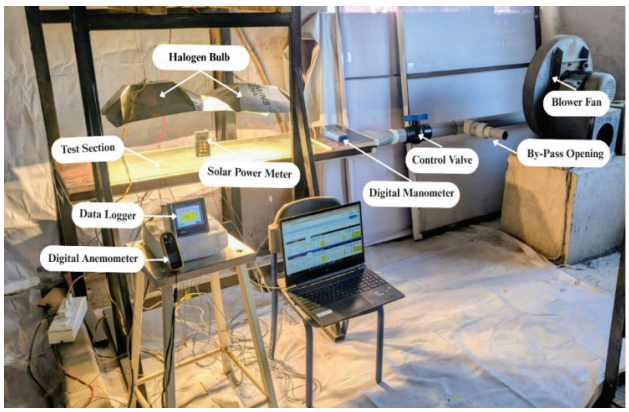

Fig. 1. Experimental Setup.

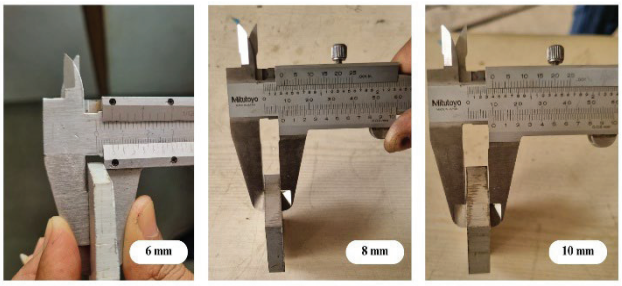

Fig. 2. Roughness rib geometrical view displaying different heights.

Fast-drying epoxy was employed to attach the roughness ribs securely to the bottom of the absorber sheet. Table 2 presents the system and operating parameters utilized in the experiment. The parameter p/e = 10 was selected based on the ideal value presented in the literature review.

The layout includes essential components such as a power blower, a halogen bulb, a digital anemometer (Model: GM816), a digital pressure gauge, a galvanized iron pipe, control valves, a data logger, and calibrated thermocouples. Temperatures were measured at various locations using RTD (PT-100) thermocouples connected to a data logger. The experiment sought to gather data on the friction factor and heat flow by employing various blockage ratios and angles of attack. We examined various roughness parameters to ensure that the major components, including the digital data logger, digital manometer, and digital anemometer, functioned properly.

For each roughened sheet, five flow rate measurements were obtained and subsequently adjusted using control valves. All values were recorded following the adjustment of the flow rate and the stabilization of the system. During the experiment, we documented the air and plate temperatures, pressure drops in the duct, and readings from the digital manometer. "Quasi-steady state" denotes the condition in which the temperature of the absorber plate and the air outlet remain constant for a duration of twenty minutes. During the initial stages, each test run required approximately two to three hours to achieve a steady state. Depending on the

measured parameter and the particular operating conditions, the total experimental error is predicted to be between ±2% and ±5% when taking into account the unique uncertainties of the instruments used.

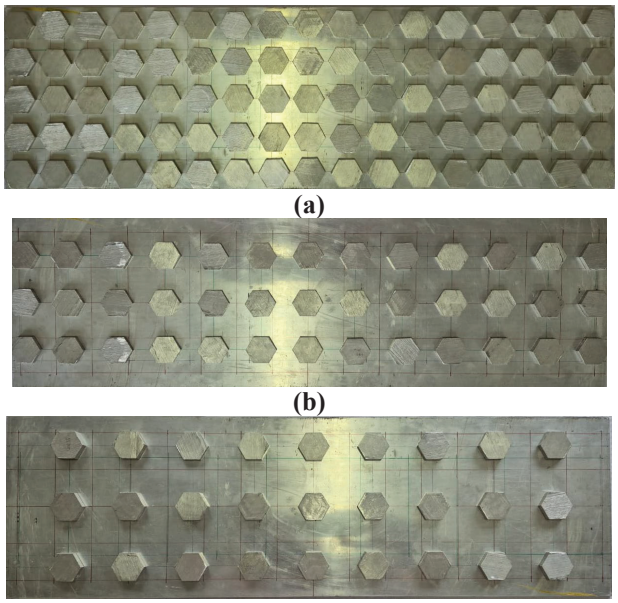

(a) (b) (c)

Fig. 3. Inline arrangement for a) 120 Degree e/D_h= 0.1849 b) 120 Degree e/D_h= 0.1479 c) 120 Degree e/D_h= 0.1109.

OPERATING PARAMETERS FOR EXPERIMENT

Device	Typical Uncertainty
Digital Anemometer	±2 % – ±5 % of reading
Digital Manometer	±1 % – ±2 % of reading
Data Logger	±0.5 ◦C – ±0.1 ◦C
3-phase AC Motor + Blower	Minor speed Fluctuation
Selector Switch, Control Valve, GI Pipe, Duct Sections	Negligible direct uncertainty

III. EXPERIMENTAL DATA ANALYSIS

Various tools were employed to document the experimental readings for different roughness components with varying blockage ratios on the absorber plate. The data obtained from the rough sheet and the smooth sheet were analyzed following the adjustment of the air flow rate via a control valve. The Nusselt number, friction factor, heat transfer coefficient, and thermo-hydraulic performance (THP) were calculated based on the experimental data obtained.

A. Data Reduction

i. Mean temperature of plate (T_{pm})

$$T_{pm} = \frac{T_1+T_2+T_3+T_4+T_5+T_6+T_7+T_8+T_9+T_{10}+T_{11}}{11} \quad (1)$$

ii. Average temperature of bulk air (T_{fm})

$$T_{fm} = \frac{T_i + T_0}{2} \quad (2)$$

iii. Hydraulic Diameter (D_h)

$$D_h = \frac{4 \times W \times H}{2 \times (W+H)} \quad (3)$$

iv. Heat gained by air (Q)

$$Q = \dot{m} C_p (T_0 - T_i) \quad (4)$$

v. Convective heat transfer coefficient from Newton's Law of Cooling

$$h = \frac{Q}{A_p (T_{pm} - T_{fm})} \quad (5)$$

vi. Nusselt number

$$Nu = \frac{hD_h}{K} \quad (6)$$

vii. Friction factor

$$f = \frac{\Delta P \times D_h}{2 \times \rho \times L \times V^2} \quad (7)$$

viii. Thermo-Hydraulic Performance

$$THP = \frac{Nu/Nu_s}{(f/f_s)^{1/3}} \quad (8)$$

B. Experimental evaluation

Before collecting the actual data, the test setup was validated through trials conducted on a smooth duct. After comparing the experimental results with the theoretical outcomes from equations (9) and (10), the values of f and Nu were obtained from these trials. The Value of f for a smooth trapezoidal duct is calculated by the Modified Blasius equation:

$$f_{th} = 0.085\ (Re)^{-\frac{1}{4}} \quad (9)$$

The Value of Nu for a smooth trapezoidal duct is calculated by the Dittus-Boelter equation

$$Nu_{th} = 0.023 Re^{0.8} Pr^{0.4} \quad (10)$$

IV. RESULT AND DISCUSSION

This study experimentally examines the influence of various flow configurations and surface roughness characteristics on heat transfer during air flow in a

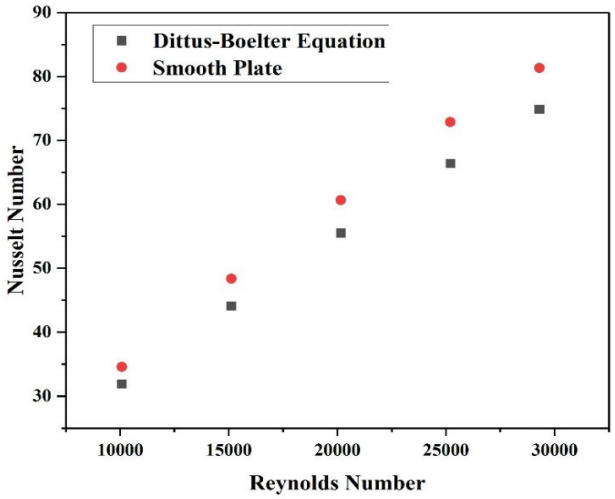

Fig. 4. Nusselt Number vs. Reynolds Number for Smooth Plate.

trapezoidal duct. The performance of various roughness parameters is compared to that of a smooth duct under similar flow conditions to evaluate improvements in h, Nu, and f. Fig. 4 illustrates the experimental trend indicating an increase in the Nusselt Number with elevated Reynolds number (Re), while Table 4 provides a summary of the documented enhancements in the heat transfer coefficient.

Figure 5 illustrates the experimental trend indicating a reduction in the Friction Factor with increasing Reynolds number (Re). Table 5 provides a summary of the reported friction factor values.

TABLE III. COMPARISON OF EXPERIMENTAL AND THEORETICAL NUSSELT NUMBERS ACROSS REYNOLDS NUMBERS FOR SMOOTH PLATE.

Sr. No	Reynolds Number	Nu_{exp}	Nu_{th}
1	10081.75	34.58	31.886
2	15122.62	48.35	44.105
3	20163.5	60.66	55.521
4	25204.37	72.87	66.374
5	29300.09	81.31	74.872

TABLE IV. COMPARISON OF EXPERIMENTAL AND THEORETICAL FRICTION FACTOR ACROSS REYNOLDS NUMBERS FOR SMOOTH PLATE.

Sr. No	Reynolds Number	Nu_{exp}	Nu_{th}
1	10081.75	0.0349	0.0316
2	15122.62	0.0316	0.0285
3	20163.5	0.0293	0.0266
4	25204.37	0.0277	0.0251
5	29300.09	0.0268	0.0242

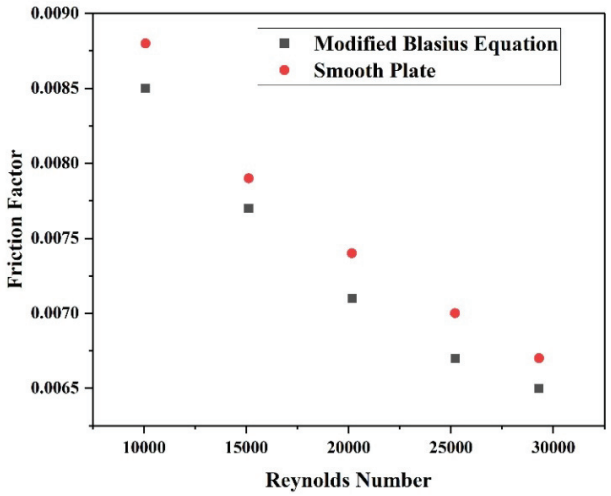

Fig. 5. Friction Factor vs Reynolds Number for Smooth plate.

A. Effect of blockage ratio on Nusselt Number

The inline ribs at α=90° exhibit a clear enhancement in Nusselt number compared to the smooth duct across all Reynolds numbers studied. From Figure 6, at a Reynolds number of approximately 10,000, the smooth duct records a Nusselt number of 34.6, whereas ribbed ducts achieve 43.1, 47.2, and 49.8 for blockage ratios of e/Dh=0.1849, 0.1479, and 0.1109, corresponding to increases of 24.6%, 36.5%, and 43.9%, respectively. At a higher Reynolds number of about 20,000, the smooth duct reaches 60.7, while the ribbed ducts improve to 69.6, 73.8, and 76.9, giving enhancements of 14.7%, 21.6%, and 26.6%, respectively. At a Reynolds number of 25,000, the trend of increasing Nusselt numbers continues. The smooth duct records 72.9, while the ribbed ducts record 81.9, 86.0, and 89.5, which are 12.4%, 18.0%, and 22.8% better. The at α=90° inline arrangement raises the Nusselt number by 16.4%, 23.8%, and 29.3% on average for the three blockage ratios. This study shows that higher rib heights always lead to more turbulence and better heat transfer performance.

The inline ribs at α=120° exhibit a clear enhancement in Nusselt number compared to the smooth duct across all Reynolds numbers studied. Figure 7 illustrates this clearly. At a Reynolds number of around 10,000, the Nusselt number of the smooth duct is 34.6, while ribbed ducts achieve 58.4, 65.9, and 70.2 for blockage ratios of e/Dh=0.1109, 0.1479, and 0.18490, corresponding to increases of 68.8%, 90.5%, and 103%, respectively. At a Reynolds number of 20,000, the smooth duct records 60.7, whereas the ribbed ducts produce 84.8, 92.4, and 97.2, resulting in enhancements of 39.6%, 52.2%, and 60.1%. At higher flow rates near 25,000 Reynolds numbers, the smooth duct value of 72.9 increases to 97.2, 104.7, and 109.8 for ribbed ducts, giving 33.4%, 43.6%, and 50.6% gains, respectively. On average, the α=120° orientation yields 44.6%, 58.1%, and 66.8% higher Nusselt numbers for the three blockage ratios, confirming its superior ability to disrupt the thermal boundary layer and sustain higher turbulence intensity.

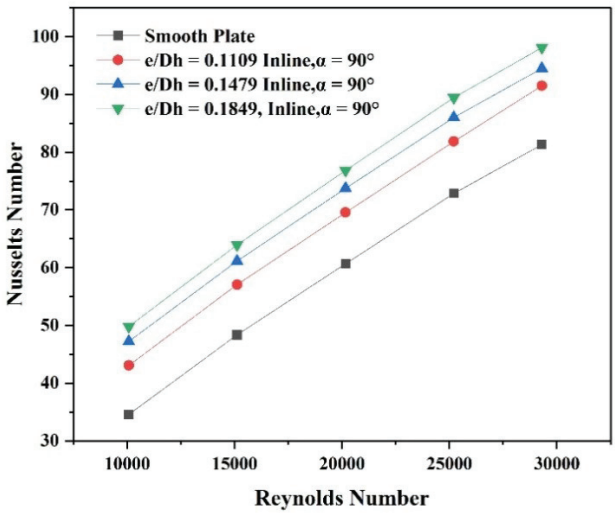

Fig. 6. Nusselt Number vs. Reynolds Number for 90-degree inline ribs with different blockage ratio.

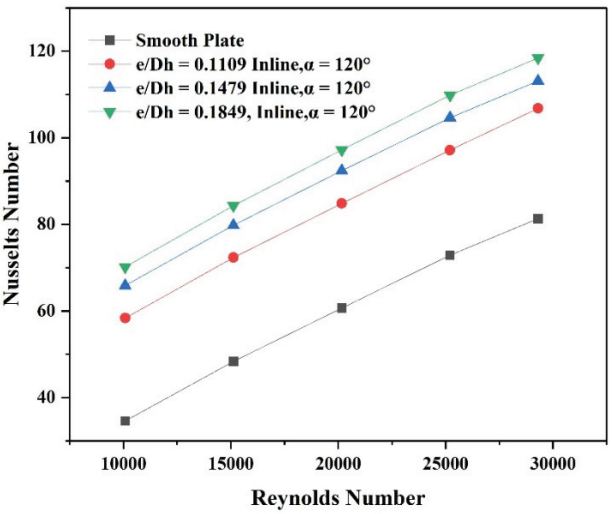

Fig. 7. Nusselt Number vs. Reynolds Number for 120-degree inline ribs with different blockage ratio.

The findings from experiments indicate that rib-roughened ducts considerably improve convective heat transfer relative to smooth ducts in inline designs. For all rib geometries examined (e/Dh = 0.1109, 0.1479, 0.1849). The Nusselt number consistently increases with the Reynolds number for attack angles of 90° and 120°, indicating the beneficial impact of flow acceleration on heat transfer enhancement in the figure.8. Quantitative research indicates that for ribs oriented at 90°, the average enhancement over the smooth duct is around 16.4%, 23.8%, and 29.3% for e/Dh = 0.1109, 0.1479, and 0.1849; and 0.1849, respectively. The enhancement is more significant for ribs oriented at 120°, with corresponding improvements of 44.6%, 58.1%, and 66.8%. The figure clearly illustrates the enhanced thermal performance of inclined ribs, with the 120° orientation yielding more pronounced flow disturbances and greater boundary layer disruption. Consequently, ribbed ducts, especially with elevated blockage ratios and sloped orientations, provide significant thermo-hydraulic advantages and are well-suited for applications like solar air heaters and compact heat exchangers.

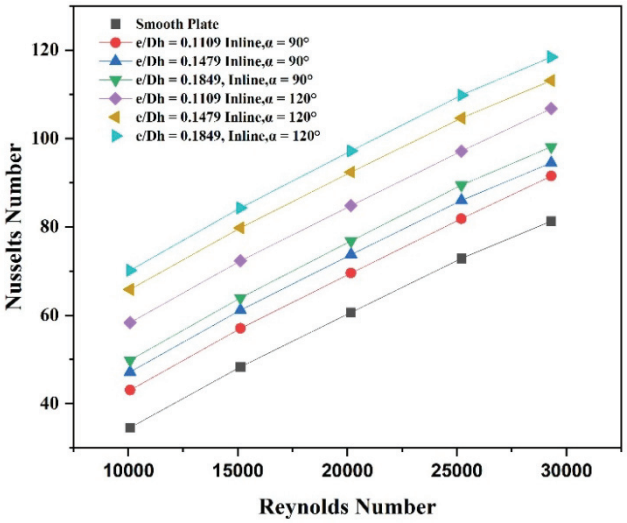

Fig. 8. Nusselt Number vs. Reynolds Number for 90-degree and 120-degree inline ribs with different blockage ratio.

B. Effect of blockage ratio on Friction Factor

The comparison of friction factors between smooth and ribbed ducts at α=90° inline configurations indicates a noticeable increase in flow resistance with the introduction of ribs. At a Reynolds number of 10,081, the smooth plate exhibits a friction factor of 0.0088, whereas ribbed ducts record values of 0.017, 0.018, and 0.020 for e/Dh=0.1109,0.1479, and 0.1849, representing increases of approximately 93%, 105%, and 127%, respectively. As the Reynolds number increases to 20,163, the friction factor of the smooth plate reduces to 0.0074, while ribbed ducts show 0.0105, 0.0115, and 0.0135, corresponding to enhancements of 42%, 55%, and 82%. At the highest Reynolds number of 29,300, the smooth plate reaches 0.0067, compared to ribbed ducts with 0.0097, 0.0107, and 0.0127, yielding 45%, 60%, and 90% increments. On average, the α=90° inline ribs increase friction factors by ~60–100%, with the effect more pronounced at higher rib heights.

The friction factor for ducts with ribs inclined at α=120° is consistently higher than that of the smooth duct. At a Reynolds number of 10,081, the smooth duct has a friction factor of 0.0088, whereas the ribbed ducts register 0.0185, 0.0195, and 0.0215 for e/Dh=0.1109,0.1479, and 0.18490, which correspond to increments of 110%, 122%, and 144%, respectively. At 20,163 Reynolds number, the smooth duct value of 0.0074 increases to 0.012, 0.013, and 0.015, giving enhancements of 62%, 76%, and 103%. Similarly, at the highest Reynolds number of 29,300, the friction factor of the smooth duct is 0.0067, while ribbed ducts exhibit 0.0113, 0.0123, and 0.0143, resulting in increases of 69%, 84%, and 113%, respectively. Overall, the α=120° inline ribs increase the friction factor by ~80–120%, with the highest blockage ratio showing the greatest penalty in flow resistance.

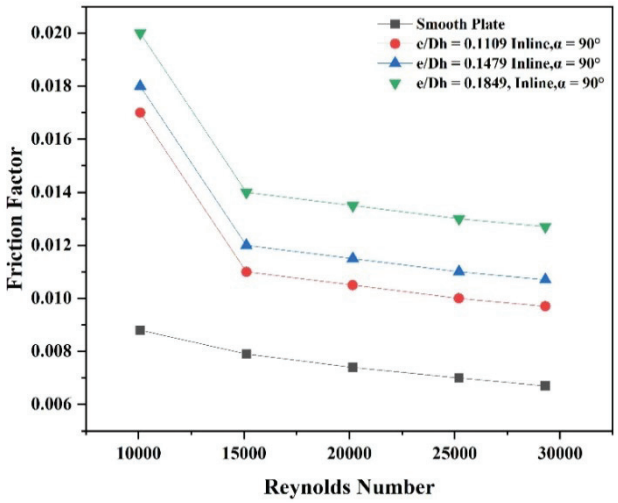

Fig. 9. Friction Factor vs. Reynolds Number for 90-degree inline ribs with different blockage ratio.

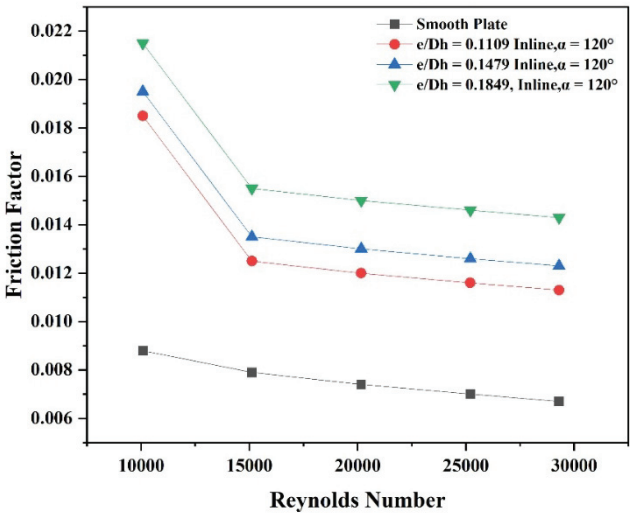

Fig. 10. Friction Factor vs. Reynolds Number for 120-degree inline ribs with different blockage ratio.

A direct comparison between the α=90° and α=120° inline ribs highlights the influence of rib orientation on flow resistance. At a Reynolds number of 10,081, the α=90° ribs increase friction factor by up to 127%, while the α=120° ribs raise it further to 144%. At 20,163 Reynolds number, the α=90° ribs produce increments of 42–82%, whereas the α=120° orientation results in higher increases of 62–103%. Even at the maximum Reynolds number of 29,300, the α=90° ribs enhance friction factor by 45–90%, while the α=120° ribs show higher increments of 69–113%. This comparison confirms that the inclined ribs at α=120° impose

a greater flow resistance than the perpendicular ribs at α=90°. While both orientations enhance turbulence and heat transfer, the additional pressure drop associated with the α=120° arrangement must be carefully considered in thermo-hydraulic performance evaluation.

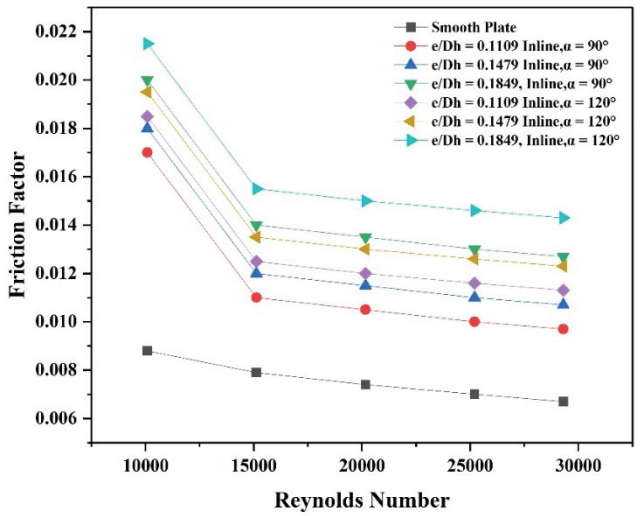

Fig. 11. Friction Factor vs. Reynolds Number for 120-degree inline ribs with different blockage ratio.

C. *Effect of blockage ratio on Thermal Performance*

The thermo-hydraulic performance factor (TPF) was evaluated to determine the combined influence of heat transfer enhancement and pressure drop penalty for both 90° and 120° inline rib configurations. From figure 12, for the 90° arrangement, TPF values remain only slightly above unity, with averages of 1.03, 1.06, and 1.05 for blockage ratios of e/Dh=0.1109,0.1479, and 0.1849, respectively. This indicates modest net gains, with peak performance of 1.11 observed at lower Reynolds numbers. In contrast, the 120° rib configuration exhibits consistently superior thermo-hydraulic performance, with average TPF values of 1.09, 1.15, and 1.15 for the corresponding blockage ratios. Notably, the maximum observed TPF of 1.29 occurs at e/Dh=0.1849e/Dh = 0.1849e/Dh=0.1849 and low Reynolds number, representing nearly a 16–18% improvement over the best-performing 90° case.

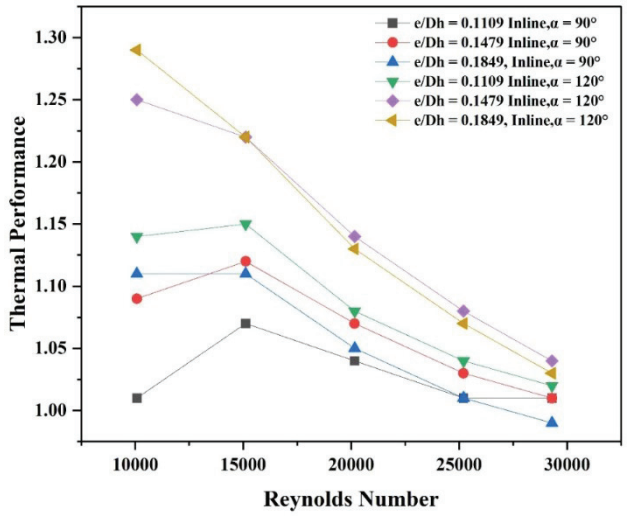

Fig. 12. Thermal Performance vs. Reynolds Number for 90-Degree and 120-degree inline ribs with different blockage ratio.

Even at higher Reynolds numbers, where TPF values generally converge toward unity, the 120° ribs maintain a measurable advantage, outperforming the 90° arrangement by approximately 6–10 percentage points across all blockage ratios. These results clearly demonstrate that rib inclination plays a decisive role in overall thermo-hydraulic efficiency, with the 120° orientation offering a more favorable balance between heat transfer augmentation and frictional losses, particularly at medium-to-high blockage ratios and low-to-moderate Reynolds numbers.

V. CONCLUSION

The present investigation on rib-roughened conduits underscores the impact of rib orientation (α = 90° and 120° inline) and blockage ratio (*e*/*Dh*=.1109,0.1479, and 0.1849), on how heat and flow go through it. Compared to the smooth duct, the Nusselt value for both ribbed variants go up a lot.

- For all Reynolds values, the α =120° inline configuration exhibits a greater increase. For instance, the Nusselt number in the α = 120° situation is almost 1.4 – 1.6 times that of the smooth plate when Re ≈10,000. It is only 1.2–1.4 times as high as the smooth plate in the α = 90° instance.
- But this advantage comes with a greater friction factor, which is particularly visible for the α =120° ribs and can be up to 2.5–3 times higher than the smooth duct values at lower Reynolds numbers.
- The thermo-hydraulic performance factor (TPF) was used to measure the combined effect, and the results revealed that the α =120° inline ribs always worked better than the α =90° configuration. The TPF values for ribs at α =90° are only a little higher than 1.03–1.06, but the values for ribs at α =120° are substantially higher, between 1.09 and 1.15. The maximum TPF of 1.29 was observed when the angle was α =120° and *e*/*Dh* = 0.1849. This is nearly 16–18% better than the best-performing α =90°.
- The results demonstrate that the α =120° inline ribs do a better job of balancing the pros and cons of more heat transfer and more friction. This makes them preferable for thermo-hydraulic optimization, especially when the blockage ratio is large and the Reynolds number is low to moderate.

A. *Future scope and applications of this study*

The proposed project holds promising potential to advance thermal management solutions across a wide range of industries. Utilizing a hexagonal geometry enhances the heat transfer rate and overall efficiency by expanding the surface area and generating secondary flows that improve fluid mixing and thermal distribution. This design can be applied in several areas, including:

- Electronics cooling systems, where effective heat dissipation is vital for optimal performance and durability.
- Industrial heat exchangers, where greater efficiency can reduce energy consumption and operational expenses.

- Automotive and aerospace applications, particularly in cooling engines and managing the thermal loads of high-performance components.
- Renewable energy technologies, by boosting the efficiency of solar thermal collectors and energy storage systems.
- HVAC systems, contributing to more sustainable and energy-efficient building designs. Future studies could focus on adapting this geometry to different scales, materials, and environmental conditions, paving the way for further advancements in the field of thermal engineering.

While various roughness parameters have been investigated, the specific effects of additional geometric configurations on heat transfer and overall system performance are still not well understood. Addressing this gap could offer valuable insights into optimizing roughness design, ultimately improving thermal performance and enabling cost-effective solutions for solar energy systems. Further studies like CFD analysis, complex ribs geometry are essential to uncover the mechanisms and advantages of multiple roughness geometries, driving progress and practical applications in the field

Appendix A. Uncertainty analysis

Experimental tests invariably entail a degree of uncertainty, regardless of the meticulousness of their execution. Consequently, it is essential to ascertain the extent to which scientific measurements may be erroneous. The error analysis was conducted to estimate the uncertainty range of the experimental data. This was accomplished by examining the dispersion of the utilized raw data. Kline and McClintock, devised a method to ascertain the ambiguity of experimental data, which is employed in this study. The error in the measurement of "y" is determined when the value of any parameter is computed using specific measured values.

$$\frac{\delta y}{y} = \left[\left(\frac{\delta y}{\delta x_1}\delta x_1\right)^2 + \left(\frac{\delta y}{\delta x_2}\delta x_2\right)^2 + \cdots \left(\frac{\delta y}{\delta x_n}\delta x_n\right)^2\right]^{0.5}$$

a. Area of the absorber plate (Ap).

$$A_P = W \times L$$

$$\frac{\delta A_P}{A_P} = \left[\left(\frac{\delta A_P}{\delta L}\delta L\right)^2 + \left(\frac{\delta A_P}{\delta W}\delta W\right)^2\right]^{0.5}$$

$$\frac{\delta A_P}{A_P} = \left[\left(\frac{\delta L}{L}\right)^2 + \left(\frac{\delta W}{W}\right)^2\right]^{0.5}$$

$$\frac{\delta A_P}{A_P} = \left[\left(\frac{0.001}{1}\right)^2 + \left(\frac{0.00003}{0.31725}\right)^2\right]^{0.5}$$

$$\frac{\delta A_P}{A_P} = 0.001004 \; or \; 0.1004\%$$

b. Area of flow (Ac).

$$\frac{\delta A_c}{A_c} = \left[\left(\frac{\delta A_P}{\delta W}\delta W\right)^2 + \left(\frac{\delta A_P}{\delta H}\delta H\right)^2\right]^{0.5}$$

$$\frac{\delta A_c}{A_c} = \left[\left(\frac{\delta W}{W}\right)^2 + \left(\frac{\delta H}{H}\right)^2\right]^{0.5}$$

$$\frac{\delta A_c}{A_c} = \left[\left(\frac{0.00003}{0.31725}\right)^2 + \left(\frac{0.00006}{0.03000}\right)^2\right]^{0.5}$$

$$\frac{\delta A_c}{A_c} = 0.00200223 \; or \; 0.2002\%$$

c. Hydraulic diameter (Dh)

$$\frac{\delta D}{D} = \left[\left(\frac{\delta D}{\delta W}\delta W\right)^2 + \left(\frac{\delta D}{\delta H}\delta H\right)^2\right]^{0.5}$$

$$\frac{\delta D}{D} = [(0.0149 \times 3 \times 10^{-5})^2 + (1.669 \times 3 \times 10^{-5})^2]^{0.5}$$

$$\frac{\delta D}{D} = 0.001827 \; or \; 0.1827\%.$$

d. Useful heat gain (Qu)

$$Q_u = m \times C_P \times (T_0 - T_i)$$

$$\frac{\delta Q_u}{Q_u} = \left[\left(\frac{\delta \dot{m}}{\dot{m}}\right)^2 + \left(\frac{\delta C_P}{C_P}\right)^2 + \left(\frac{\delta \Delta T}{\Delta T}\right)^2\right]^{0.5}$$

$$\frac{\delta Q_u}{Q_u} = [(0.01\,)^2 + (0.001)^2 + (0.0488)^2]^{0.5}$$

$$\frac{\delta Q_u}{Q_u} = 0.0498 \; or \; 4.98\%$$

e. Reynolds Number (Re)

$$\frac{\delta Re}{Re} = \left[\left(\frac{\delta \dot{m}}{\dot{m}}\right)^2 + \left(\frac{\delta \mu}{\mu}\right)^2 + \left(\frac{\delta D_h}{D_h}\right)^2\right]^{0.5}$$

$$\frac{\delta Re}{Re} = [(0.01)^2 + (0.01)^2 + (0.001827)^2]^{0.5}$$

$$\frac{\delta Re}{Re} = 0.0142 \; or \; 1.43\%$$

f. Prandtl number (Pr)

$$\frac{\delta Pr}{Pr} = \left[\left(\frac{\delta k}{k}\right)^2 + \left(\frac{\delta \mu}{\mu}\right)^2 + \left(\frac{\delta C_P}{C_P}\right)^2\right]^{0.5}$$

$$\frac{\delta Pr}{Pr} = [(0.0003694)^2 + (0.01)^2 + (0.001)^2]^{0.5}$$

$$\frac{\delta Pr}{Pr} = 0.010056 \; or \; 1.0056\%$$

g. Nusselt number (Nu)

$$\frac{\delta Nu}{Nu} = \left[\left(\frac{\delta k}{k}\right)^2 + \left(\frac{\delta h}{h}\right)^2 + \left(\frac{\delta D_h}{D_h}\right)^2\right]^{0.5}$$

$$\frac{\delta Nu}{Nu} = [(0.0003694)^2 + (0.05573)^2 + (0.001827)^2]^{0.5}$$

$$\frac{\delta Nu}{Nu} = 0.05579 \; or \; 5.579\%$$

h. Friction factor (f)

$$\frac{\delta f}{f} = \left[\left(\frac{\delta \Delta P}{\Delta P}\right)^2 + \left(\frac{\delta L}{L}\right)^2 + \left(\frac{\delta D_h}{D_h}\right)^2 + \left(2\frac{\delta V}{V}\right)^2\right]^{0.5}$$

$$\frac{\delta f}{f} = [(0.00423)^2 + (0)^2 + (0.001827)^2 + 2 \times (0.01075)^2]^{0.5}$$

$$\frac{\delta f}{f} = 0.02198 \; or \; 2.20\%$$

TABLE V. UNCERTAINTY IN THE COMPUTED PARAMETERS FOR EXPERIMENTAL DATA.

Sr. No	Parameters	Uncertainty
1	Area of the absorber plate (Ap).	0.1004%
2	Area of flow (Ac).	0.2002%
3	Hydraulic diameter (Dh)	0.1827%.
4	Useful heat gain (Qu)	4.98%
5	Reynolds Number (Re)	1.43%
6	Prandtl number (Pr)	1.0056%
7	Nusselt number (Nu)	5.579%
8	Friction factor (f)	2.20%

Abbreviations and Acronyms

Ti = Temp. of air at entry (°C)
To = Temp. of air at exit (°C)
W= Width of Duct
H= Height of Duct
ρ = density of air
V = Air velocity.
Dh = Hydraulic dia.
μ = Viscosity of air
m = Air mass flow rate (kg/s)
Cp = Specific heat of air at static pressure (kJ/kg-K)
Q = Heat gained/received by air, Watt.
Ap = Area of the absorber sheet, m^2
T_{pm} = Average Temp. of sheet, °C.
T_{fm} = Average Temp. of fluid flowing, °C
h = Convective heat transfer coefficient (W/m^2-K)
Dh = Hydraulic dia. of quadratic duct, m
k = Thermal Conductivity of the flowing fluid (W/m-K)
ΔP = Pressure drop
L= Length of duct
V= Velocity of air
Nu & Nus =Nusselt no. of rough and smooth plate
f & fs =friction factor of rough and smooth plate

Graphical Abstract

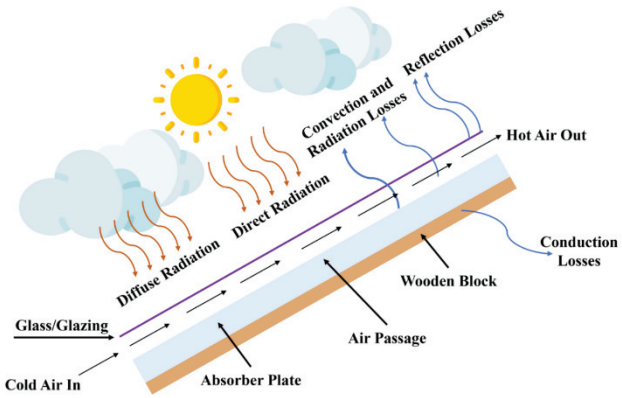

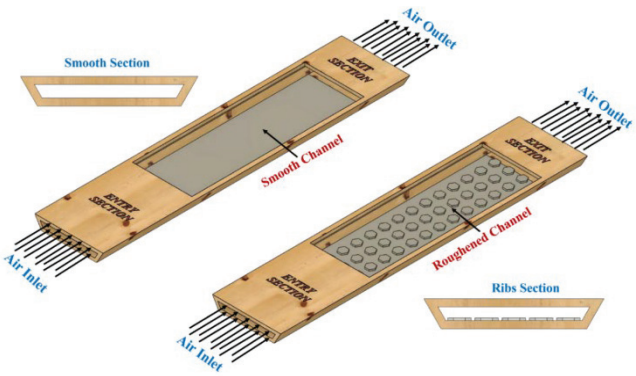

Fig 13

ACKNOWLEDGMENT

Authors gratefully acknowledged the Director, Medi-caps University, Indore for providing necessary library facilities and digital library. I am also thankful to the department of Mechanical Engineering department of Medi-caps University for helping me at various stages of this paper.

REFERENCES

[1] Alsaiari, A. O., Iqbal, A., Abdulkhair, H., Gzara, L., Almatrafi, E., Alzahrani, H. A. H., Madhukeshwara, N., Prasanna, B. M., & Aljohani, M. (2022). Heat transmission and air flow friction in a solar air heater with a ribbed absorber plate: A computational study. Case Studies in Thermal Engineering, 40, 102517. https://doi.org/10.1016/j.csite.2022.102517

[2] Ghritlahre, H., & Prasad, R. (2018). Prediction of exergetic efficiency of arc shaped wire roughened solar air heater using ANN model. International Journal of Heat and Technology, 36(3), 1107–1115. https://doi.org/10.18280/ijht.360343

[3] Kumar, R., Verma, S. K., Gupta, N. K., Mendiburu, A. Z., Sharma, A., Alam, T., & Eldin, S. M. (2023). Experimental assessment and modeling of solar air heater with V shape roughness on absorber plate. Case Studies in Thermal Engineering, 43, 102784. https://doi.org/10.1016/j.csite.2023.102784

[4] J. Nikuradse, Laws of Flow in Rough Pipes, 1292, NACA Technical Memorandum, 1950.

[5] Agrawal, Y., Bhagoria, J. L., Gautam, A., Sharma, A., Yadav, A. S., Alam, T., Kumar, R., Goga, G., Chakroborty, S., & Kumar, R. (2023). Investigation of thermal performance of a ribbed solar air heater for sustainable built environment. Sustainable Energy Technologies and Assessments, 57, 103288. https://doi.org/10.1016/j.seta.2023.103288

[6] Chabane, F., Grira, F., Moummi, N., & Brima, A. (2019). Experimental study of a solar air heater by adding an arrangement of transverse rectangular baffles perpendicular to the air stream. International Journal of Green Energy, 16(14), 1264–1277. https://doi.org/10.1080/15435075.2019.1671401

[7] Nidhul, K., Yadav, A. K., Anish, S., & Arunachala, U. C. (2022). Thermo-hydraulic and exergetic performance of a cost-effective solar air heater: CFD and experimental study. Renewable Energy, 184, 627–641. https://doi.org/10.1016/j.renene.2021.11.111

[8] Abulkhair, H., Alsaiari, A. O., Ahmed, I., Almatrafi, E., Madhukeshwara, N., & Sreenivasa, B. R. (2023). Heat transfer and air flow friction in solar air heaters: A comprehensive computational and experimental investigation with wire-roughened absorber plate. Case Studies in Thermal Engineering, 48, 103148. https://doi.org/10.1016/j.csite.2023.103148

[9] Kamali, R., & Binesh, A. R. (2008). The importance of rib shape effects on the local heat transfer and flow friction characteristics of square ducts with ribbed internal surfaces. International Communications in Heat and Mass Transfer, 35(8), 1032–1040. https://doi.org/10.1016/j.icheatmasstransfer.2008.04.012

[10] Peng, W., Jiang, P.-X., Wang, Y.-P., & Wei, B.-Y. (2011). Experimental and numerical investigation of convection heat transfer in channels with different types of ribs. Applied Thermal Engineering, 31(14–15), 2702–2708. https://doi.org/10.1016/j.applthermaleng.2011.04.040

[11] Varun Kumar, B., Manikandan, G., & Rajesh Kanna, P. (2021). Enhancement of heat transfer in SAH with polygonal and trapezoidal shape of the rib using CFD. Energy, 234, 121154. https://doi.org/10.1016/j.energy.2021.121154

[12] Karmveer, Kumar Gupta, N., Alam, T., & Singh, H. (2024). An Experimental Study of Thermohydraulic Performance of Solar Air Heater Having Multiple Open Trapezoidal Rib Roughnesses. Experimental Heat Transfer, 37(3), 313–333. https://doi.org/10.1080/08916152.2022.2139024

[13] Yadav, A. S., & Bhagoria, J. L. (2014). A CFD based thermo-hydraulic performance analysis of an artificially roughened solar air heater having equilateral triangular sectioned rib roughness on the absorber plate. International Journal of Heat and Mass Transfer, 70, 1016–1039. https://doi.org/10.1016/j.ijheatmasstransfer.2013.11.074

[14] Kumar, R., Verma, S. K., Gupta, N. K., Mendiburu, A. Z., Sharma, A., Alam, T., & Eldin, S. M. (2023). Experimental assessment and modeling of solar air heater with V shape roughness on absorber plate. Case Studies in Thermal Engineering, 43, 102784. https://doi.org/10.1016/j.csite.2023.102784

[15] Mahanand, Y., & Senapati, J. R. (2020). Thermal enhancement study of a transverse inverted-T shaped ribbed solar air heater. International Communications in Heat and Mass Transfer, 119, 104922.https://doi.org/10.1016/j.icheatmasstransfer.2020.104922

[16] Patel, Y. M., Jain, S. v., & Lakhera, V. J. (2021). Thermo-hydraulic performance analysis of a solar air heater roughened with discrete reverse NACA profile ribs. International Journal of Thermal Sciences, 167, 107026. https://doi.org/10.1016/j.ijthermalsci.2021.107026

[17] Mahanand, Y., & Senapati, J. R. (2022). Thermo-fluid analysis of a pentagonal ribbed triangular solar air heater duct (TSAHD): A three-dimensional numerical investigation. International Communications in Heat and Mass Transfer, 137, 106258. https://doi.org/10.1016/j.icheatmasstransfer.2022.106258

[18] Dutt, N., Hedau, A. J., Kumar, A., Awasthi, M. K., Singh, V. P., & Dwivedi, G. (2023). Thermo-hydraulic performance of solar air heater having discrete D-shaped ribs as artificial roughness. Environmental Science and Pollution Research. https://doi.org/10.1007/s11356-023-28247-9

[19] Nidhul, K., Kumar, S., Yadav, A. K., & Anish, S. (2020). Enhanced thermo-hydraulic performance in a V-ribbed triangular duct solar air heater: CFD and exergy analysis. Energy, 200, 117448. https://doi.org/10.1016/j.energy.2020.117448

[20] Hans, V. S., Saini, R. P., & Saini, J. S. (2010). Heat transfer and friction factor correlations for a solar air heater duct roughened artificially with multiple v-ribs. Solar Energy, 84(6), 898–911. https://doi.org/10.1016/j.solener.2010.02.004

[21] Jin, D., Quan, S., Zuo, J., & Xu, S. (2019). Numerical investigation of heat transfer enhancement in a solar air heater roughened by multiple V-shaped ribs. Renewable Energy, 134, 78–88. https://doi.org/10.1016/j.renene.2018.11.016

[22] Bekele, A., Mishra, M., & Dutta, S. (2014). Performance characteristics of solar air heater with surface mounted obstacles. Energy Conversion and Management, 85, 603–611. https://doi.org/10.1016/j.enconman.2014.04.079

[23] Nanjundappa, M. (2020). Optimum thermo-hydraulic performance of solar air heater provided with cubical roughness on the absorber surface. Experimental Heat Transfer, 33(4), 374–387. https://doi.org/10.1080/08916152.2019.1652214

[24] Antony, A. L., Shetty, S. P., Madhwesh, N., Yagnesh Sharma, N., & Vasudeva Karanth, K. (2020). Influence of stepped cylindrical turbulence generators on the thermal enhancement factor of a flat plate solar air heater. Solar Energy, 198, 295–310. https://doi.org/10.1016/j.solener.2020.01.065

[25] Arunkumar, H. S., Kumar, S., & Karanth, K. V. (2020). Analysis of a solar air heater for augmented thermohydraulic performance using helicoidal spring shaped fins-A numerical study. Renewable Energy, 160, 297–311. https://doi.org/10.1016/j.renene.2020.06.098

[26] Bezbaruah, P. J., Das, R. S., & Sarkar, B. K. (2021). Experimental and numerical analysis of solar air heater accoutered with modified conical vortex generators in a staggered fashion. Renewable Energy, 180, 109–131. https://doi.org/10.1016/j.renene.2021.08.046

[27] Saravanan, A., Murugan, M., Reddy, M. S., Ranjit, P. S., Elumalai, P. V., Kumar, P., & Sree, S. R. (2021). Thermo-hydraulic performance of a solar air heater with staggered C-shape finned absorber plate. International Journal of Thermal Sciences, 168, 107068. https://doi.org/10.1016/j.ijthermalsci.2021.107068

[28] Sharma, S. L., Kishor, K., Bisht, V. S., Debbarma, A., & Gaur, A. (2024). CFD analysis of artificially roughened solar air heater: a comparative study of C-Shape, reverse C-Shape, and reverse R-Shape roughness element. International Journal of Ambient Energy, 45(1). https://doi.org/10.1080/01430750.2024.2331240

[29] Azadani, L. N., & Gharouni, N. (2021). Multi objective optimization of cylindrical shape roughness parameters in a solar air heater. Renewable Energy, 179, 1156–1168. https://doi.org/10.1016/j.renene.2021.07.084

[30] Alzahrani, H. A. H., Danappa, G. T., Anantha Prasad, M. G., Rajesh, K., al Jadidi, S., Madhukeshwara, N., & Prasanna, B. M. (2023). Enhancing solar air heater efficiency with 3D cylinder shaped roughness elements. Case Studies in Thermal Engineering, 51, 103617. https://doi.org/10.1016/j.csite.2023.103617

[31] Alsaiari, A. O., Alzahrani, H. A. H., N, M., & Prasanna, B. M. (2022). Heat transfer augmentation in a solar air heater with conical roughness elements on the absorber. Case Studies in Thermal Engineering, 36, 102210. https://doi.org/10.1016/j.csite.2022.102210

[32] Kumar, V., & Murmu, R. (2023). Performance based investigation of inclined spherical ball roughened solar air heater. Applied Thermal Engineering, 224, 120033. https://doi.org/10.1016/j.applthermaleng.2023.120033